Cosmic-Ray Rejection by Laplacian Edge Detection

Pieter G. van Dokkum[1]
California Institute of Technology, MS 105-24, Pasadena, CA 91125
pgd@astro.caltech.edu

Accepted for publication in the PASP

ABSTRACT

Conventional algorithms for rejecting cosmic-rays in single CCD exposures rely on the contrast between cosmic-rays and their surroundings, and may produce erroneous results if the Point Spread Function (PSF) is smaller than the largest cosmic-rays. This paper describes a robust algorithm for cosmic-ray rejection, based on a variation of Laplacian edge detection. The algorithm identifies cosmic-rays of arbitrary shapes and sizes by the sharpness of their edges, and reliably discriminates between poorly sampled point sources and cosmic-rays. Examples of its performance are given for spectroscopic and imaging data, including *Hubble Space Telescope* WFPC2 images.

Subject headings: instrumentation: detectors — methods: data analysis — techniques: image processing

1. Introduction

Various methods are in use for identifying and replacing cosmic-ray hits in CCD data. The most straightforward approach is to obtain multiple exposures of the same field (or multiple non-destructive readouts during a single exposure; e.g., Fixsen et al. 2000). In general, a given pixel will suffer from a cosmic-ray hit in only one or two of the exposures, and remaining exposures can be used to obtain its replacement value (e.g., Zhang 1995). Methods for combining multiple exposures have reached a high degree of sophistication, particularly those developed for dithered *Hubble Space Telescope* (HST) data (e.g., Windhorst, Franklin, & Neuschaefer 1994, Freudling 1995, Fruchter & Hook 1997).

However, there are circumstances when cosmic-ray identification in single exposures is required or desirable. The object of interest may be varying or moving on short timescales, and in the case of long-slit spectra the positions and intensities of sky lines and object spectra may change (e.g., Croke 1995). Furthermore, pixels can be hit by cosmic-rays in more than one exposure, and some affected pixels may remain after combining individual images. Cosmic-ray removal in individual exposures may also be desirable if the images are shifted with respect to each other by a non-integer number of pixels, or if the seeing varied significantly between the exposures (see Rhoads 2000). Finally, multiple exposures are simply not always available.

Methods for identifying cosmic-rays in single images or spectra include median filtering (e.g., Qzap by M. Dickinson), filtering by adapted Point Spread Functions (PSFs) (e.g., Rhoads 2000), trained neural networks (Salzberg et al. 1995), and interpolation of neighbouring pixels (e.g., the Cosmicrays task in the IRAF package). All these methods effectively remove small cosmic-rays from well sampled data.

The most widely used methods are based on some form of median filtering, and usually include adaptations to exclude stars and emission lines from the list of cosmic-rays. However, problems arise when cosmic-rays affect more than half the area of the filter, or the PSF is smaller than the filter. The size of the filter is therefore a trade-off between detecting large cosmic-rays and limiting contamination by structure on the scale of the PSF.

In this paper, a new algorithm for rejecting

[1]Hubble Fellow

cosmic-rays in single exposures is described. It is based on Laplacian edge detection, which is a widely used method for highlighting boundaries in digital images (see, e.g., Gonzalez & Woods 1992). The strength of the method is that it relies on the sharpness of the *edges* of cosmic-rays rather than the contrast between entire cosmic-rays and their surroundings. Therefore, it is largely independent of the morphology of cosmic-rays. This property is very useful, and forms the basis for a robust discrimination between poorly sampled point sources and cosmic-rays.

2. The Laplacian

The Laplacian of a 2-D function is a second-order derivative defined as

$$\nabla^2 f = \frac{\partial f}{\partial x^2} + \frac{\partial f}{\partial y^2}. \tag{1}$$

The Laplacian is commonly used for edge detection in digital images. In this application the image is convolved with the Laplacian of a 2-D Gaussian function of the form

$$f(x, y) = \exp\left(-\frac{r^2}{2\sigma^2}\right), \tag{2}$$

where $r^2 \equiv x^2+y^2$ and σ is the standard deviation. The second-order derivative with respect to r has the form

$$\nabla^2 f = \left(\frac{r^2 - 2\sigma^2}{\sigma^4}\right) \exp\left(-\frac{r^2}{2\sigma^2}\right). \tag{3}$$

The Laplacian has zero-crossings at $r = \pm\sqrt{2}\sigma$, and the locations of edges are found by identifying zero-crossings in the convolved image. The standard deviation can be tuned to the smoothness of the edge, and by using a range of values for σ both sharp and smooth edges can be identified (Marr & Hildreth 1980).

Cosmic-rays have very sharp edges, and the convolution kernel should be most sensitive to variations on small scales. The appropriate discrete implementation of Eq. 3 has the form

$$\nabla^2 f = \frac{1}{4} \left\{ \begin{array}{rrr} 0 & -1 & 0 \\ -1 & 4 & -1 \\ 0 & -1 & 0 \end{array} \right\}. \tag{4}$$

The average value of a Laplacian image (obtained by convolving an image with the kernel given in Eq. 4) is zero, and smooth structure in the image is removed.

3. Implementation

3.1. Basic Procedure

A straightforward convolution of Eq. 4 with a CCD image produces negative cross patterns around high pixels. As a result, connected cosmic-ray pixels suffer from attenuation by the negative cross patterns of their neighbors. Hence before convolution the original image I needs to be subsampled. The results are independent of the subsampling factor, and a factor two is computationally least expensive:

$$I^{(2)}_{i,j} = I_{\mathrm{int}([i+1]/2),\mathrm{int}([j+1]/2)}, \tag{5}$$

with $n \times n$ the size of the original image and $i, j = 1, \ldots, 2n$. The Laplacian of the subsampled image is

$$\mathcal{L}^{(2)} = \nabla^2 f \circ I^{(2)}, \tag{6}$$

with $\circ$ denoting convolution.

The Laplacian of the edge of a cosmic-ray is negative on the outside and positive on the inside of the cosmic-ray. Therefore, by setting all negative values in the Laplacian image to zero cosmic-ray affected pixels are retained and their negative cross patterns are removed:

$$\mathcal{L}^{(2)+} = \begin{cases} \mathcal{L}^{(2)} & \text{if} \quad \mathcal{L}^{(2)} \geq 0 \\ 0 & \text{if} \quad \mathcal{L}^{(2)} < 0 \end{cases} \tag{7}$$

Finally, the image is resampled to its original resolution:

$$\mathcal{L}^{+}_{i,j} = \frac{1}{4}\left(\mathcal{L}^{(2)+}_{2i-1,2j-1} + \mathcal{L}^{(2)+}_{2i-1,2j} + \mathcal{L}^{(2)+}_{2i,2j-1} + \mathcal{L}^{(2)+}_{2i,2j}\right), \tag{8}$$

with $i, j = 1, \ldots, n$.

The process is illustrated in Fig. 1. A small section of a 2D long slit spectrum is shown in (a). Panel (b) shows the same image, subsampled by a factor six and convolved with the Laplacian kernel given in Eq. 3. Edges are at the locations of zero-crossings. In panel (c) all negative values are set to zero. Finally, the image is block averaged by a factor six (panel d). The cosmic-ray stands out clearly. Because the spectrum is smooth on scales of ~ 1 pixel its Laplacian is close to zero.

The numerical value associated with each edge is the difference between the two neighbouring pixels, and the resampled Laplacian of an image I

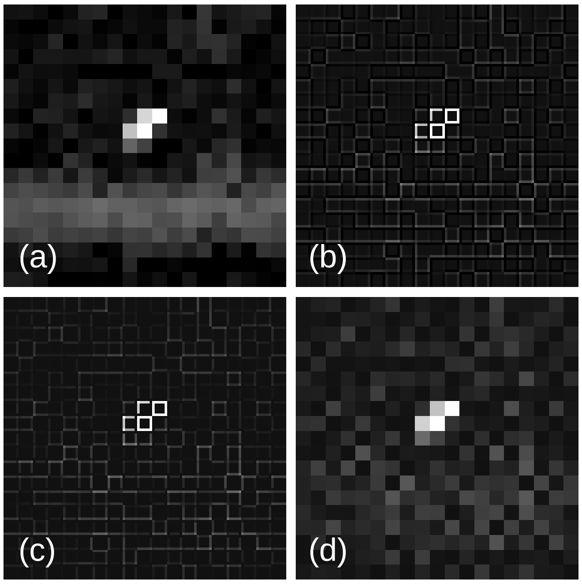

Fig. 1.— Illustration of Laplacian edge detection. The original image is shown in (a). Panel (b) shows the same image after subsampling by a factor six and convolution with the Laplacian kernel. Edges are positive on the inside of the cosmic-ray, and negative on the outside. Negative pixels are set to zero in (c), and the image is block averaged to its original resolution in (d).

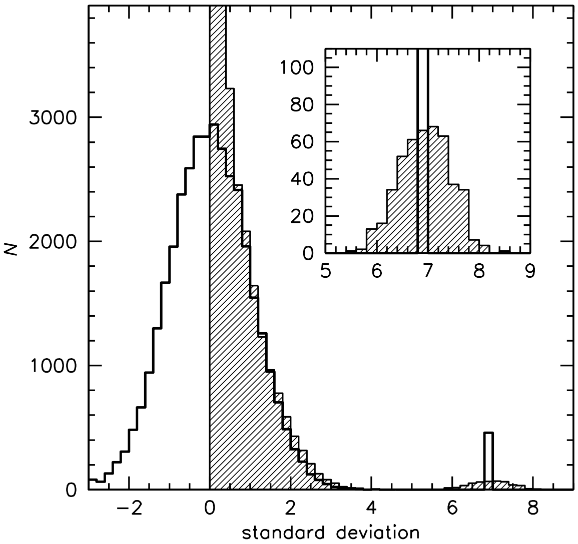

Fig. 2.— The thick solid line shows the noise properties of a simulated image with $\sim 10^3$ 7σ cosmic-rays. The hatched histogram shows the distribution of pixel values in the Laplacian image. Pixel values in the Laplacian image were divided by the subsampling factor. In the positive tail of the noise distribution the characteristics of the original image are (to a good approximation) conserved. The width of the distribution of cosmic-rays is increased by 0.5σ.

consisting of a smooth background B with superposed noise and cosmic-rays is approximately

$$\mathcal{L}^+ \sim \begin{cases} f_s(I-B) & \text{if} \quad I-B \geq 0 \\ 0 & \text{if} \quad I-B < 0 \end{cases} \tag{9}$$

with f_s the subsampling factor that was used. The Laplacian thus retains the flux in high pixels and removes the local background, making it very useful for identifying cosmic-rays.

To identify cosmic-rays in the Laplacian image the value of each pixel is compared to the expected noise at that location. The noise characteristics of the Laplacian image are not the same as in the original image: the Laplacian operator itself increases the noise by a factor $\sqrt{5/4}$, and all negative Poisson fluctuations in the original image are (close to) zero in the Laplacian image. These effects are demonstrated in Fig. 2 for a simulated image containing $\sim 10^3$ 7σ cosmic-rays. As expected, the distribution of pixel values near zero is strongly distorted by the Laplacian. However, the positive tail of the distribution (i.e., the region where cosmic-rays are found) remains virtually unchanged. Therefore the noise properties of the original image can be used for identifying cosmic-rays in $\mathcal{L}^+$, which greatly simplifies the analysis.

The noise model is constructed by convolving the original image with a median filter:

$$N = g^{-1}\sqrt{g\,(M_5 \circ I) + \sigma_{rn}^2}, \tag{10}$$

where g is the gain in electrons/ADU, σ_{rn} is the readnoise in electrons, and M_5 is a 5×5 median filter. For long slit spectroscopic data the algorithm offers the option of fitting and subtracting sky lines and/or object spectra. These fits provide the basis for the long slit noise model, which is optimized by applying Eq. 10 to the residuals from the fits.

The Laplacian image is divided by the noise model to obtain the deviations from the expected Poisson fluctuations:

$$S = \frac{\mathcal{L}^+}{f_s N}. \tag{11}$$

Cosmic-rays are identified by selecting pixels in S that are above a given threshold $\sigma_{\rm lim}$.

For single-pixel cosmic-rays on a smooth background the detection probability depends on the noise in the background $\sigma_{\rm org}$ only. The error in the background estimate scales as $\sigma_{\rm org}/\sqrt{n}$, with n the number of pixels. Since four neighbouring pixels are used to determine the Laplacian of a given pixel, the width of the distribution of cosmic-rays is increased by $\sigma_{\rm org}/2$ (see Fig. 2). As an example, if a detection threshold of 5σ is applied, $\sim 5\,\%$ of 4σ peaks in the original image will be marked as cosmic-rays, $\sim 50\,\%$ of 5σ peaks, and $\sim 95\,\%$ of 6σ peaks.

The detection probability of cosmic-rays larger than a single pixel depends on the number of connected pixels and the pixel-to-pixel variation within the cosmic-ray. In general the Laplacian (and hence the detection probability) is lowest for cosmic-rays with small pixel-to-pixel variations. In the limiting case of a cosmic-ray with negligible pixel-to-pixel variation

$$S_{i,j} \sim N_{i,j}^{-1}\left(1-\frac{n_{i,j}}{4}\right)(I_{i,j}-B_{i,j}), \qquad (12)$$

with $n_{i,j}$ the number of cosmic-ray pixels adjacent to pixel (i,j). Pixels on the corners of large cosmic-rays have at most two adjacent pixels, and the Laplacian always retains at least $\approx 50\,\%$ of their flux. Therefore, (arbitrarily) large cosmic-rays can be removed by applying the rejection process iteratively. Before each iteration, pixels flagged as cosmic-rays in previous iterations are replaced by the median of surrounding "good" pixels.acd

3.2. Removal of Sampling Flux

The Laplacian gives the difference between one pixel and its neighbours, and contains no information on the nature of detected features. Real astronomical objects produce signal in the Laplacian image because of Poisson noise and because their intrinsically smooth intensity profiles are sampled by the pixels. This "sampling flux" is generally small, and will not produce spurious detections as long as it does not exceed the predicted Poisson fluctuations (see Eq. 10, 11). However, for bright objects the sampling flux can be significant, in particular if the Point Spread Function (PSF) is not well sampled.

Sampling flux is removed from S in two steps. First, all structure that is smooth on scales of $\gtrsim 5$ pixels is removed by a 5×5 median filter:

$$S' = S - (S \circ M_5). \qquad (13)$$

This procedure very effectively removes sampling flux resulting from extended bright objects (including point sources if the PSF is well sampled). Because of the large size of the filter cosmic-rays and the noise properties of S remain unaffected.

Next, sampling flux resulting from critically sampled (or even undersampled) point sources is removed. As is well known, it is very hard to distinguish cosmic-rays from stars and emission lines in marginally sampled data, because they can have very similar pixel-to-pixel variations within an area $\lesssim 3\times 3$ pixels.

Point sources are distinguished from cosmic-rays by their symmetry. An image only containing symmetric fine structure on scales of $2-3$ pixels is constructed and compared to the Laplacian image. This "fine structure image" $\mathcal{F}$ is created from the original image by a combination of median filters:

$$\mathcal{F} = (M_3 \circ I) - ([M_3 \circ I] \circ M_7)\,, \qquad (14)$$

where M_n is an $n\times n$ median filter. The second term serves to remove large scale structure from $\mathcal{F}$. An important property of $\mathcal{F}$ is that central pixels of undersampled point sources do not vanish, but are replaced by the median of the surrounding pixels. The Laplacian image is divided by the fine structure image, and cosmic-rays are selected as those pixels which have $S' > \sigma_{\rm lim}$ *and* $\mathcal{L}^+/\mathcal{F} > f_{\rm lim}$, with $f_{\rm lim}$ defining the minimum contrast between the Laplacian image and the fine structure image.

Figure 3 demonstrates the procedure. Artificial images of three stars and a cosmic-ray are shown in the top row. One stellar image is slightly oversampled ($\sigma = 1.5$ pixels), the second is critically sampled ($\sigma = 1.0$ pixels), and the third is slightly undersampled ($\sigma = 0.7$ pixels). The contrast between the cosmic-ray and its local background is identical to the contrast between the central pixel of the undersampled star and its local background. As a result, the highest pixels in their Laplacian images $\mathcal{L}^+$ (shown in the second row) have very similar values. The third row shows fine structure images $\mathcal{F}$. The cosmic-ray has very low signal in $\mathcal{F}$, whereas the stars retain a significant fraction of their flux because of their symmetry. The bottom row shows the Laplacian images divided by the fine structure, $\mathcal{L}^+/\mathcal{F}$. Only pixels with $\mathcal{L}^+/\mathcal{F} > f_{\rm lim}$ are retained. The critically sampled star has $\mathcal{L}^+/\mathcal{F} = 0.7$, and $\mathcal{L}^+/\mathcal{F} = 1.8$ for the undersampled star. The cosmic-ray has $\mathcal{L}^+/\mathcal{F} = 21$, and is easily distinguished from undersampled point sources.

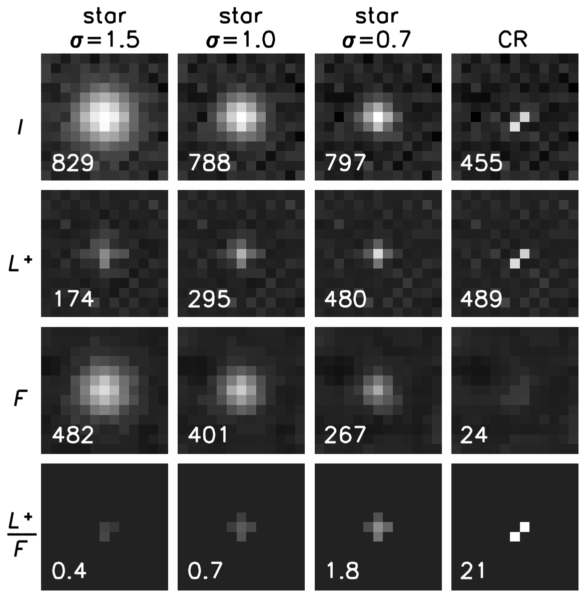

Fig. 3.— Differentiating between marginally sampled point sources and cosmic-rays. Panels show, from top to bottom, artifical images of stars and a cosmic-ray, the Laplacian of these images $\mathcal{L}^+$, their fine structure image $\mathcal{F}$, and the Laplacian divided by the fine structure $\mathcal{L}^+/\mathcal{F}$. The number in each panel is the value of the highest pixel. The highest pixels in the Laplacian images of the undersampled star ($\sigma = 0.7$ pixels) and the cosmic-ray are similar. However, they are very different after division by the fine structure image.

In general, the appropriate value of $f_{\rm lim}$ depends on the sampling of a given point source, its S/N ratio, and whether it lies on the center of a pixel or close to the edge. These effects can be simulated by creating artificial PSFs with varying sampling, S/N ratios, and subpixel positions, and calculating $\mathcal{L}^+/\mathcal{F}$ for each star. Figure 4 shows the dependence of $\mathcal{L}^+/\mathcal{F}$ on the sampling, expressed as the full width at half maximum (FWHM) of stars (in pixels). The width of the shaded region demonstrates the (maximum) effects of varying S/N ratio and subpixel position.

These simulations demonstrate that the value of $\mathcal{L}^+/\mathcal{F}$, and hence the appropriate choice of $f_{\rm lim}$, depends mainly on the sampling. For data that are well sampled $f_{\rm lim} = 2$ is appropriate; hence this is the default value in the algorithm. For undersampled data higher values of $f_{\rm lim}$ are needed to discriminate point sources and cosmic-rays; as an example, data taken with the Wide Field chips in HST's WFPC2 camera require $f_{\rm lim} \approx 5$.

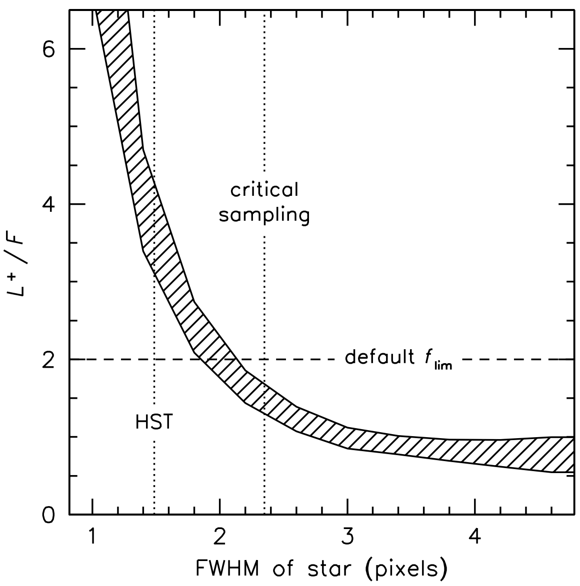

Fig. 4.— Dependence of the ratio of the Laplacian $\mathcal{L}^+$ and the fine structure image $\mathcal{F}$ on the sampling, as derived from simulations (see text). For a given FWHM of stars the value of $f_{\rm lim}$ should be chosen such that it exceeds the dashed band. The default $f_{\rm lim} = 2$ is appropriate for data that are critically, or better, sampled. HST WFPC2 data require $f_{\rm lim} \approx 5$.

3.3. Additional Features

The basic algorithm detects cosmic-rays and rejects point sources from the initial list. In addition, the program L.A.Cosmic allows a lower detection threshold to be used for pixels neighbouring those already flagged as cosmic-rays. It also replaces cosmic-rays by the median of surrounding "good" pixels, and offers the option of applying the algorithm iteratively. On a Sun UltraSparc 1 (200 MHz) the IRAF implementation of L.A.Cosmic requires approximately 65 s per iteration for an image of 800×800 pixels. The run time scales linearly with the number of pixels.

4. Examples

The algorithm was tested on a variety of real and artificial data sets, consistently producing very good results. The examples given here serve to illustrate its performance.

4.1. Well Sampled Imaging CCD Data

Figure 5(a) shows a well sampled artifical image containing 500 stars, 100 galaxies, and 227 cosmic-rays. Stars have $\sigma = 1.5$ pixels, equivalent to, for example, FWHM $= 0\farcs78$ seeing with $0\farcs22$ pixels. All cosmic-rays are $\geq 5\sigma$ above the sky background. The reconstruction by L.A.Cosmic is shown in (b). Panel (c) shows the input cosmic-ray image, and panel (d) shows the cosmic-rays found by L.A.Cosmic. The program found 222 of the 227 cosmic-rays (98 %). Importantly, only 1 of the 500 stars (0.2 %) and none of the galaxies was inadvertently identified as a cosmic-ray.

For well sampled imaging data the performance is similar to median filtering methods such as Qzap (by M. Dickinson). Sophisticated median filtering recovers close to 100 % of cosmic-rays that are smaller than the filter size, but breaks down if the cosmic-ray is larger than the filter, and/or the FWHM of the PSF is smaller than the filter.

4.2. HST WFPC2 Data

Cosmic-rays in images obtained with WFPC2 on HST are notoriously difficult to remove, because of their large number and the undersampling of the PSF. Nevertheless, the algorithm described here performs very well on WFPC2 data. The method is insensitive to the size of cosmic-rays, and the undersampling of the PSF can be taken into account by setting the parameter $f_{\rm lim} = 5$ (see Sect. 3.2).

Figure 6(a) shows part of a 2400 s WF observation in I_{F814W} of galaxy cluster MS 1137+67. The reconstruction of the image by L.A.Cosmic is shown in (b).

Virtually all cosmic-rays are removed, and none of the real objects is mistaken for a cosmic-ray. The small panels show examples of stars and galaxies in WF chips, extracted from WFPC2 observations of various targets. The algorithm leaves stars intact, and is able to remove arbitrarily large cosmic-rays.

The reliability of cosmic-ray identification can be tested by comparing the results of L.A.Cosmic on single images to "true" cosmic-ray images created from multiple exposures. The test used one of the CR–SPLIT WFPC2 images of the cluster MS 2053–04 ($z = 0.58$). As a result of its low Galactic latitude approximately 50 % of $I_{\rm F814W} < 22$ objects are stars. The reduction of these data is described in van Dokkum et al. (2001). The algorithm found 5638 (98.1 %) of 5750 cosmic-ray affected pixels deviating more than 6σ from the background, and 4687 (99.1 %) of 4729 pixels deviating more than 10σ. The number of false positives, i.e., pixels inadvertently marked as cosmic-rays, is 72 (1.2 %) at $\geq 6\sigma$, and only 1 (0.02 %) at $\geq 10\sigma$. These numbers compare favorably to cosmic-ray rejection algorithms based on morphological classification by neural networks (Salzberg et al. 1995).

4.3. Spectroscopic CCD Data

The algorithm optimized for spectroscopic long-slit data is very similar to the implementation for imaging data. The main difference is that the program offers the possibility of fitting and subtracting sky lines and the object spectrum before convolution with the Laplacian kernel.

An example (an 1800 s long slit spectrum of a galaxy, obtained with the Low Resolution Imaging Spectrograph on the W. M. Keck Telescope) is shown in Fig. 7. Note that the Laplacian is very effective in removing the fringe pattern that is present after subtracting strong sky lines. The fine structure image $\mathcal{F}$ is used to identify emission lines and other sharp features in the spectra, in similar fashion as the identification of undersampled stars in imaging data.

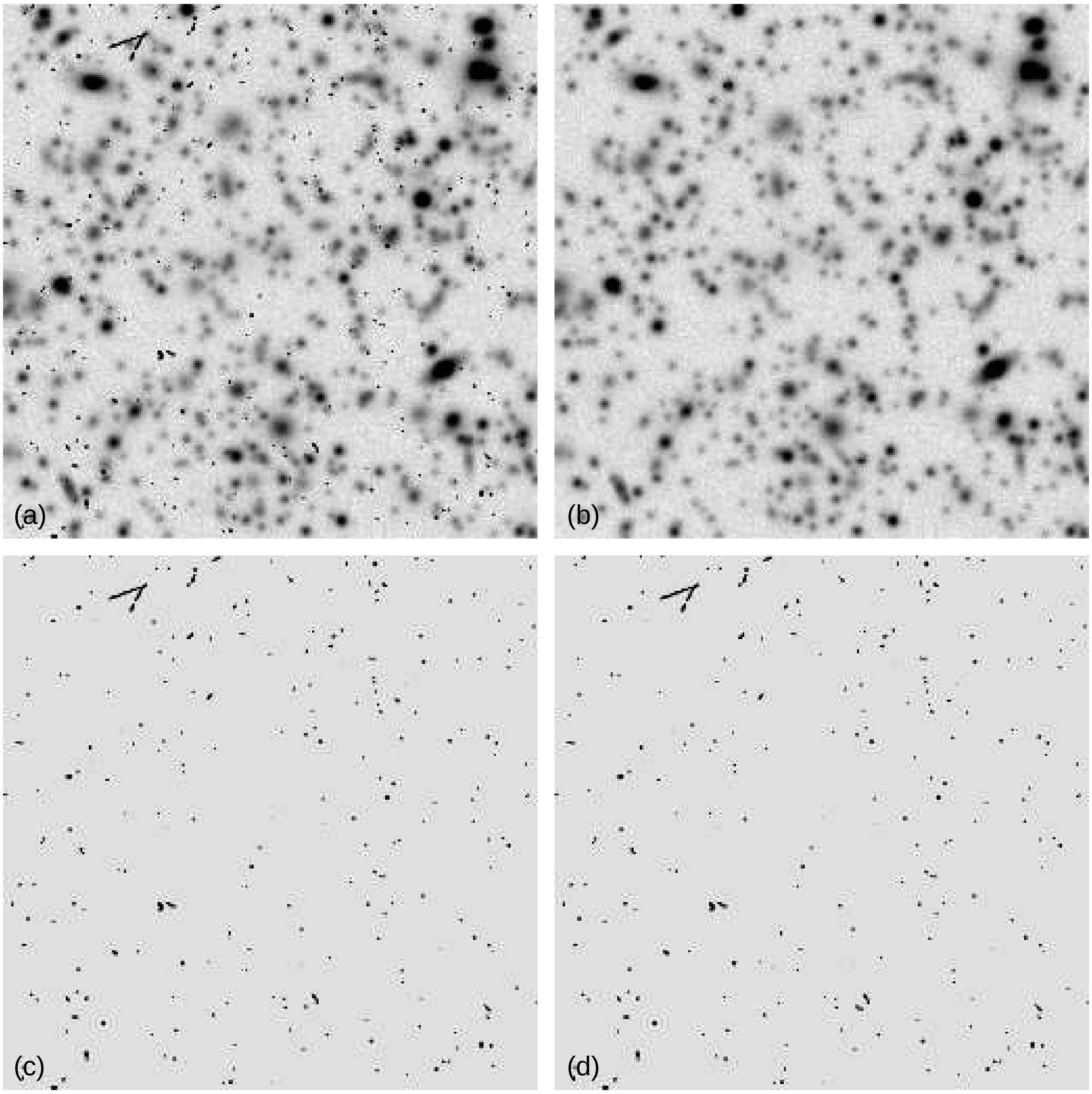

Fig. 5.— (a) Artificial image containing 500 stars, 100 galaxies, and 227 cosmic-rays. (b) Reconstruction of the image by L.A.Cosmic. The true cosmic-ray image is shown in (c), and the cosmic-rays found by L.A.Cosmic are shown in (d).

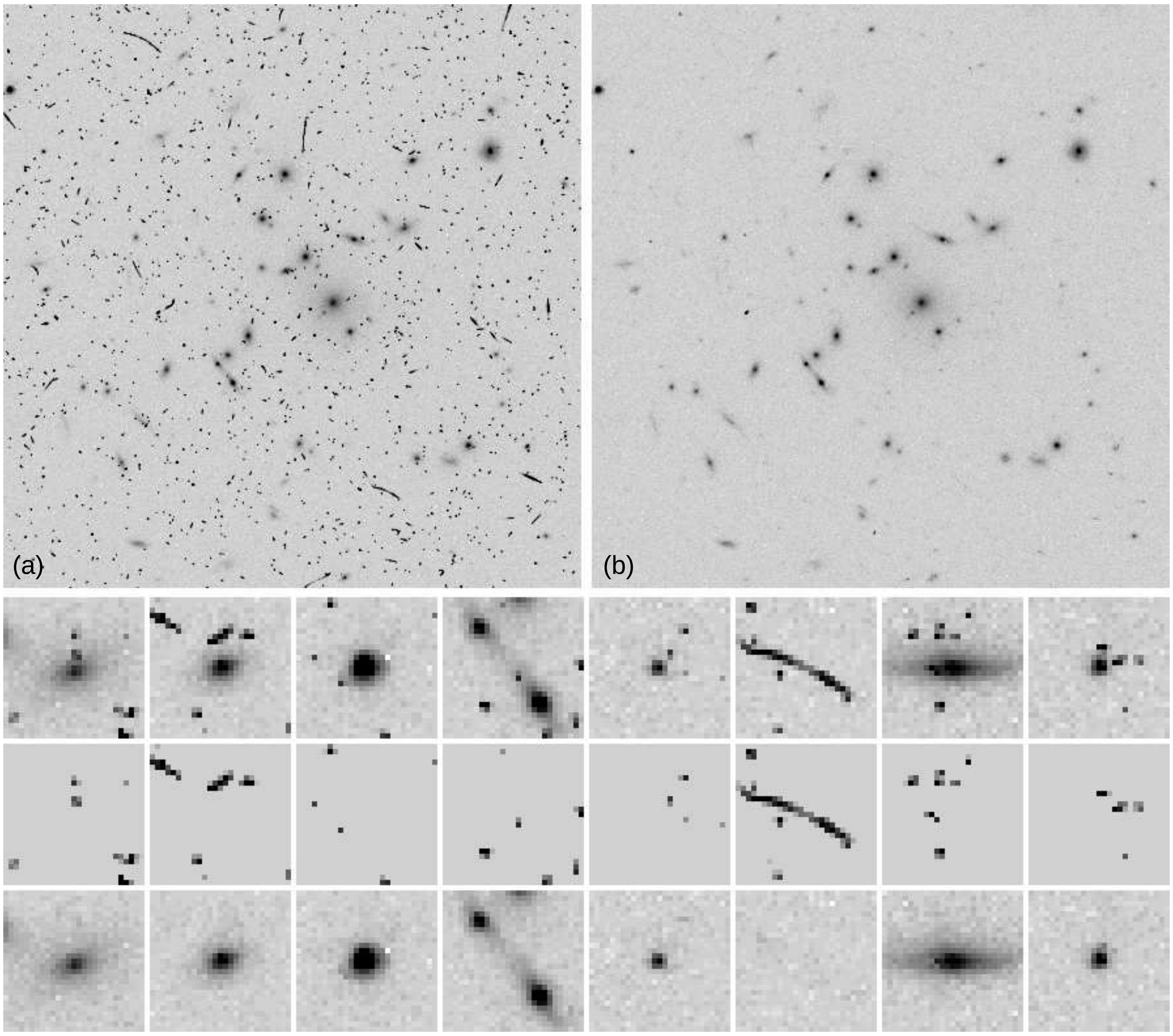

Fig. 6.— (a) HST WFPC2 image of galaxy cluster MS 1137+67. The restoration by L.A.Cosmic is shown in (b). Small panels show close-ups for a selection of stars and galaxies in various WFPC2 images. The algorithm leaves stars intact, and is able to remove cosmic-rays of arbitrary shapes and sizes.

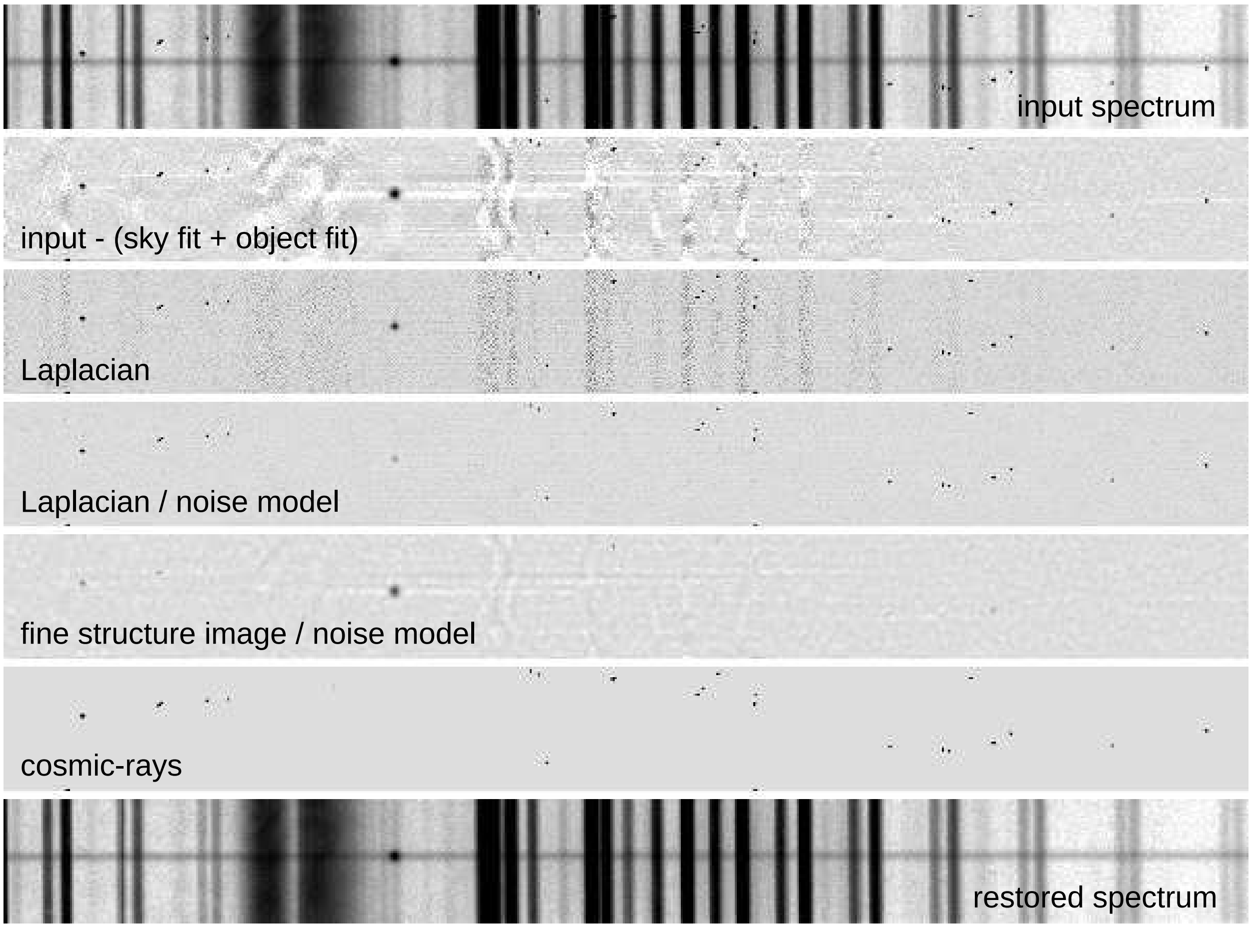

Fig. 7.— Demonstration of Laplacian cosmic-ray rejection for long-slit spectra. From top to bottom are shown: the original spectrum, the residuals after subtraction of 1D-fits to the sky lines and the object spectrum, the Laplacian image, the Laplacian image divided by the noise model, the finestructure image, the bad pixel map, and the restored spectrum. Note that the Laplacian very effectively removes fringing. In this case all cosmic-rays are removed in a single iteration. The bright emission line is not marked as a cosmic-ray because of its prominence in the fine structure image.

5. Conclusions

Cosmic-rays in single images or spectra can be removed by a variation of Laplacian edge detection. The procedure is robust, and requires very few user-defined parameters. The method rejects cosmic-rays of arbitrary size and distinguishes undersampled point sources from cosmic-rays with high confidence. It is implemented in the program L.A.Cosmic, which can be obtained from http://www.astro.caltech.edu/~pgd/lacosmic/ .

I thank Martin Zwaan for his contributions in the initial phase of this study, and Josh Bloom for discussion and comments. The insightful comments and suggestions of the referee, James Rhoads, improved the paper. The author acknowledges support by NASA through Hubble Fellowship grant HF-01126.01-99A awarded by the Space Telescope Science Institute, which is operated by the Association of Universities for Research in Astronomy, Inc., for NASA under contract NAS 5-26555.

REFERENCES

Croke, B. F. W. 1995, PASP, 107, 1255

Fixsen, D. J., Offenberg, J. D., Hanisch, R. J., Mather, J. C., Nieto-Santisteban, M. A., Sengupta, R., & Stockman, H. S. 2000, PASP, 112, 1350

Freudling, W. 1995, PASP, 107, 85

Fruchter, A. S., & Hook, R. N. 1997, in Applications of Digital Image Processing XX, A. G. Tescher, Ed., SPIE, p. 120

Gonzalez, R. C., & Woods, R. E. 1992, Digital Image Processing (Reading, Addison-Wesley)

Marr, D., & Hildreth, E. 1980, Proc. R. Soc. Lond., B207, 187

Rhoads, J. E. 2000, PASP, 112, 703

Salzberg, S., Chandar, R., Ford, H., Murthy, S. K., & White, R. 1995, PASP, 107, 279

van Dokkum, P. G., Franx, M., Kelson, D. D., & Illingworth, G. D. 2001, ApJ, 553, L39

Windhorst, R. A., Franklin, B. E., & Neuschaefer, L. W. 1994, PASP, 106, 798

Zhang, C. Y. 1995, in Astronomical Data Analysis Software and Systems IV, ASP Conference Series, Vol. 77, R. A. Shaw, H. E. Payne, and J. J. E. Hayes, eds., p. 514.

This 2-column preprint was prepared with the AAS LaTeX macros v5.0.